Metal-Organic Frameworks on Palladium Nanoparticle–Functionalized Carbon Nanotubes for Monitoring Hydrogen Storage

Sean I. Hwang,<sup>†</sup> Emmy M. Sopher,<sup>†</sup> Zidao Zeng,<sup>†</sup> Zachary M. Schulte,<sup>†</sup> David L. White,<sup>†</sup> Nathaniel L. Rosi,<sup>†</sup>, § Alexander Star<sup>†</sup>, ‡,\*

†Department of Chemistry, University of Pittsburgh, PA 15260, United States

<sup>‡</sup>Department of Bioengineering, University of Pittsburgh, Pittsburgh, Pennsylvania 15261, United States

§Department of Chemical & Petroleum Engineering, University of Pittsburgh, Pittsburgh, Pennsylvania 15261, United States

\*Corresponding author email: astar@pitt.edu

Keywords: Metal organic framework, single-walled carbon nanotubes, sensors, hydrogen storage, HKUST-1, palladium nanoparticles, chemiresistor

## **Abstract**

Palladium is a well-known hydrogen absorbing material. When palladium is functionalized with HKUST-1 (copper(II) benzene-1,3,5-tricarboxylate), a hydrogen adsorbing metal organic framework, its hydrogen absorption capacity can be increased. In this work, we show that by

growing the HKUST-1 on palladium nanoparticle functionalized single-walled carbon nanotubes (Pd NP/SWCNT), we can dynamically monitor the adsorption and desorption of hydrogen from the HKUST-1 and Pd NP composite by using the carbon nanotubes as transducers in chemiresistors. Addition of HKUST-1 to the Pd NP/SWCNT was shown to increase sensitivity of the nanocomposite material to hydrogen by 300% and limit of detection to hydrogen by 33%. The increase in sensitivity was attributed to the increased hydrogen sorption capacity of the combined HKUST-1/Pd NP. A factor of 8 improvement in sensitivity was further achieved by using semiconductor enriched SWCNT instead of mixed metallic/semiconducting nanotubes and a corresponding improvement in the theoretical limit of detection down to 70 ppb.

#### Introduction

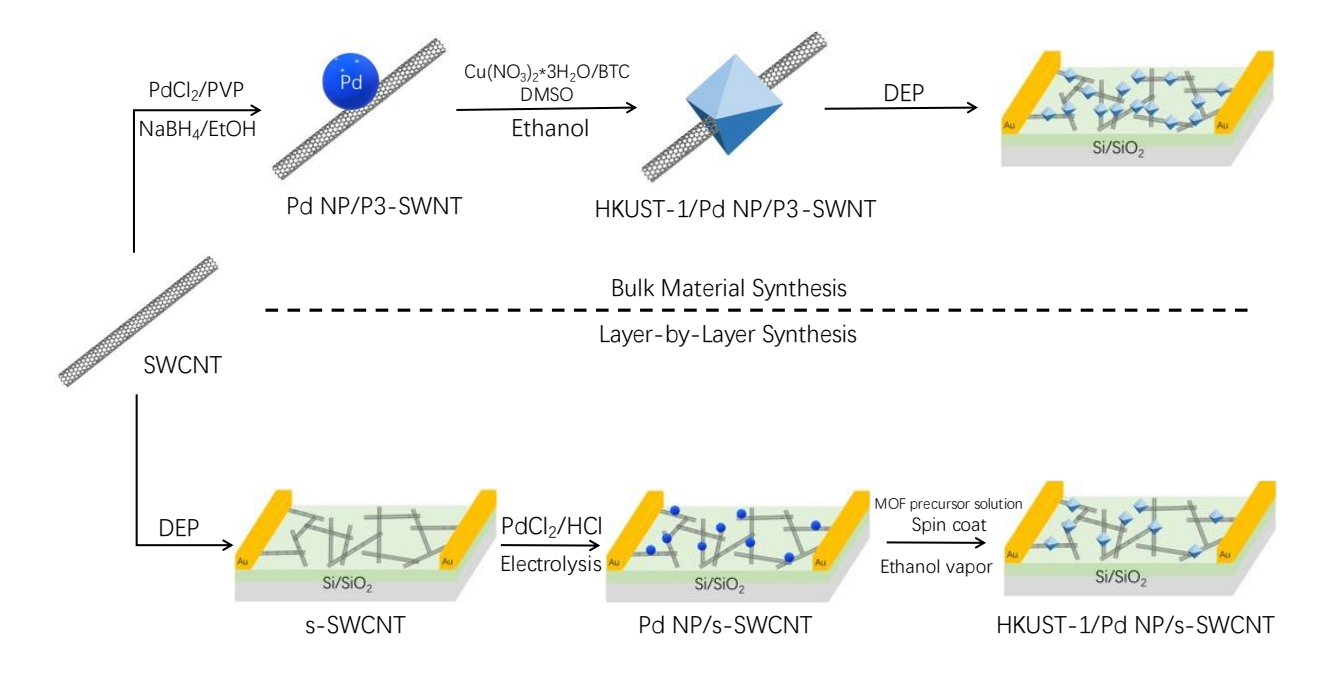
Metal organic frameworks (MOF) with their three-dimensional porous structure and large internal surface area are excellent materials for adsorbing gases. Their capability and capacity to adsorb specific types of gases can be fine-tuned by selectively choosing the organic linker and metal ion chemistry. This selective gas adsorption property makes MOF well-suited for gas phase applications such as storage, catalysis, separation, and sensing. To study its gas adsorption property, the MOF is exposed to a gas and the weight-gain of the MOF is measured as a function of the partial pressure of the applied gas to generate adsorption isotherms. In this work, we show that by growing the MOF HKUST-1 (Cu(II) benzene-1,3,5-tricarboxylate) on a known hydrogen sensitive material, palladium nanoparticle (Pd NP) functionalized single-walled carbon nanotubes (SWCNT), 2-15 we can dynamically monitor the adsorption and desorption of hydrogen from the HKUST-1 and Pd NP.

SWCNT were used to serve two purposes. One is that they are excellent transducers that are sensitive to small changes in their local charge environment. <sup>16-19</sup> The changes in the chemical potential around the nanotubes can be measured as changes in their resistance, therefore the nanotubes function as chemiresistors. Nanotubes on their own generally lack selectivity toward target analytes. Forming covalent bonds with other nanomaterials such as Pd NP enable the composite material to function as a selective chemiresistor, which in this case is hydrogen. <sup>20-22</sup> By using such hybridization strategy to form nanocomposites, nanotubes can detect analytes that they are not innately sensitive to. <sup>12</sup>

The second purpose of the nanotubes is to make the MOF composite electrically conductive. Most MOF are electrically insulating but to use them as electrocatalysts<sup>23</sup> and sensors<sup>24-26</sup> electrical conductivity is necessary property. There are two general strategies to increase the electrical conductivity of MOF. The metal and linker chemistry can be tuned to incorporate conductive pathways through the MOF with redox active linkers and extended conjugated network,<sup>27</sup> or the MOF can be combined with conductive material such as 1 dimensional carbon nanotubes and 2-dimensional MXenes (metal carbides, nitrides, or carbonitrides).<sup>28-33</sup> The combination of MOF and carbon nanotubes have previously been shown to combine the best of these two properties and form nanocomposites that have high electrical conductivity of carbon nanotubes and the high absorption capacity of MOF including synergetic improvement in gas adsorption capacity.<sup>34-35</sup>

# **Experimental Methods**

**Scheme 1.** Outline of the steps used to synthesize the bulk and layer-by-layer materials and fabricate the sensor devices.



# **Bulk Material Synthesis**

# **Palladium Nanoparticle Functionalization on SWCNT**

200 mg of oxidized single-walled carbon nanotubes (P3-SWNT Carbon Solutions) were dispersed in 200 mL of ethanol (Decon Labs) using a bath sonicator for 1 hour. 16.7 mg of PdCl<sub>2</sub> (Fisher Scientific) were dissolved in the nanotube solution to generate a 5 wt% Pd solution. 13.5 mg of polyvinylpyrrolidone (PVP, MW = 20,000, Sigma Aldrich) was then added to the solution and stirred for 1 hour. The PVP subunit was equimolar to the Pd. To reduce the Pd<sup>2+</sup> ions, 22 mg (10× molar excess to Pd) of NaBH<sub>4</sub> (Fisher Scientific) dissolved in 5 mL of ethanol was added dropwise to the Pd/nanotube solution and stirred overnight. 36-37 The composite was then filtered through 0.45  $\mu$ m pore size 47 mm nylon membrane, washed 3 times with ethanol, and then resuspended in 200 mL of ethanol.

# **HKUST-1 Functionalization on PdNP@SWCNT**

A room temperature method was used to synthesize the HKUST-1.<sup>38</sup> 1.22 g of Cu(NO<sub>3</sub>)<sub>2</sub>\*3H<sub>2</sub>O (Sigma Aldrich) and 0.693 g of 1,3,5-benzenetricarboxylic acid (BTC) (Sigma Aldrich) were placed into a beaker containing 5 mL of DMSO to make the MOF precursor solution (1 M Cu<sup>2+</sup>, 0.66 M BTC). To a vigorously stirring 100 mL of the Pd NP/ox-SWCNT solution, 56 μL of the HKUST-1 precursor solution was added and stirred for an hour. The HKUST/Pd NP/ox-SWCNT composite was left to precipitate out and approximately 90 mL of ethanol solution was decanted. 90 mL of ethanol was added and stirred vigorously to resuspend the composite. After the composite precipitated out, 90 mL of ethanol was again decanted. This washing process was repeated 2 more times. The bulk material was stored in ethanol to prevent the hydrolysis of the HKUST-1.

## **Layer-by-Layer Synthesis**

# **Carbon Nanotube Deposition on Gold Interdigitated Electrodes**

 $10~\mu g/mL$  of IsoSol-S100 SWCNT in toluene (NanoIntegris) or P3-SWNT in water was deposited on the silicon chip using dielectrophoresis ( $10~V_{pp}$ , 100~kHz, 2~minutes). The IsoSol-S100 deposited devices were washed with isopropyl alcohol, and the P3 deposited devices were washed with water. The devices were then blown dry with nitrogen and annealed in an oven at  $120^{\circ}$ C for one hour.

#### **Palladium Nanoparticle Functionalization**

Pd NP were functionalized on the nanotubes through bulk electrolysis.  $^{39}$  100  $\mu$ L of 1 mg/mL PdCl<sub>2</sub> in 0.1 M HCl (Fisher Scientific) was placed on the nanotube deposited chip. The Pd<sup>2+</sup> was reduced on the nanotubes using a 3-electrode setup with the nanotubes deposited chip as the working electrode, platinum wire as a counter electrode, and Ag/AgCl reference electrode. A constant potential was held at -0.3 V for 30 seconds on the working electrode. The device was then rinsed with deionized water, dried with nitrogen, and annealed in an oven at 120°C for one hour. The chip was then incubated with 10  $\mu$ L of 1 mg/mL PVP for one hour to functionalize the surface of the Pd NP and then rinsed with DI water.

#### **HKUST-1 Functionalization**

 $5~\mu L$  of the precursor solution was spun coat on the surface of the Pd NP/SWCNT chip at 5,000~rpm for 1 minute. The chip was then incubated in an ethanol vapor bath over night to seed and grow HKUST-1.

# **Hydrogen Sensing**

Chemiresistive sensors were fabricated from the hybrid materials to test their hydrogen sensing capability. The materials were deposited on 4 pairs of gold interdigitated electrodes lithographed on a 2 × 2 mm silicon die, which was wire bonded and potted with PDMS into a dual inline 40-pin ceramic package. The two materials were tested for hydrogen sensitivity in a custom-made gas flow by recording the changes in the current of the devices under constant 50 mV. During the sensing experiment, the devices were first purged with dry nitrogen at a flow rate of 1,000 sccm. Then the sensors were exposed to 10 minutes long pulses of hydrogen at 10, 25, 100, 10,000, 25,000, and 100,000 ppm at an increasing concentration. These concentrations were generated

using mass flow controllers by diluting a 100 ppm and 100,000 ppm hydrogen balanced in nitrogen into a gas stream of nitrogen. After the final hydrogen exposure, the sensors were purged with dry nitrogen for an hour.

## **Electron Microscopy**

The transmission electron microscopy (TEM) images were captured using a FEI Morgagni microscope operating at an acceleration voltage of 80 keV. The scanning electron microscopy (SEM) images were taken using a SEM ZEISS Sigma500 VP microscope operating at an accelerating voltage of 3 kV.

# **Power X-Ray Diffraction**

Powder X-Ray diffractogram was obtained using a Bruker D8 XRD system equipped with LynxEye detector. The bulk materials were drop-cast and dried onto a glass slide for analysis.  $2\theta$  angles between  $22^{\circ}$  and  $80^{\circ}$  were scanned at  $0.04^{\circ}$  intervals at a rate of 0.4 seconds/point. The X-ray source used was Cu K $\alpha$  held at 40 kV and 40  $\mu$ A utilizing a 0.2 mm aperture slit width.

## **Gas Adsorption Studies**

Gas adsorption isotherms were collected on a Micromeritics 3-Flex gas adsorption analyzer. Approximately 50 mg of sample was added into a pre-weighed sample analysis tube. All samples were degassed at 150°C under vacuum for 14 hours. A liquid N<sub>2</sub> bath was used for the N<sub>2</sub> adsorption studies at 77 K. During H<sub>2</sub> adsorption experiments, a water/ethylene glycol circulating bath (Huber Minichiller 300) was used to maintain a temperature of 303 K. Ultra-high purity H<sub>2</sub> gas (99.999%, Matheson Tri-gas) and N<sub>2</sub> were used for adsorption studies. All pore size distributions were generated using the Micromeritics 3-Flex Share software. A N<sub>2</sub> adsorption model with cylindrical pore geometries and an oxide surface was run through the non-local density functional theory (NLDFT) subprogram to calculate the pore size distribution.

# **Inductively Coupled Plasma Optical Emission Spectrometry**

Elemental microanalysis was performed by the University of Illinois Urbana-Champaign Microanalysis Laboratory with a PerkinElmer 2000DV ICP-OES for metal analysis.

#### **Results and Discussion**

# **Material Synthesis and Characterization**

The high-resolution transmission electron microscopy (HRTEM) micrographs of the Pd NP functionalized nanotubes (Figure S1) showed Pd NP particles with diameters on the order of 3-5 nm. The small sizes can be attributed to rapid reduction of Pd<sup>2+</sup> with borohydride. Bundles of ox-SWCNT were clearly visible in the micrograph. The mild strength of the bath sonication was not sufficient to completely separate the bundles into individual nanotubes.

HKUST-1 was grown onto the Pd NP/SWCNT using a room temperature synthesis protocol.<sup>38</sup> The TEM and SEM images of the HKUST-1 functionalized material showed both bead-on-a-string morphology and aggregated crystals (Figure 1a and c). HRTEM images of the material showed dense number of Pd NP embedded inside the HKUST-1 (Figure S2). MOF functionalization on SWCNT have previously been shown to yield bead-like structure when MOF nucleation is initiated on the nanotubes as opposed to an aggregated structure that is observed when nucleation and growth occurs in solution away from the nanotube surface.<sup>29</sup> PVP ligands on the Pd NP also served as nucleation sites for HKUST-1.<sup>40</sup> The observed crystalline structures in the TEM and SEM were confirmed to be HKUST-1 through X-ray powder diffraction (XRD) (Figure 1b) with an expected pore width of 9 Å by 9 Å (Figure 1d).

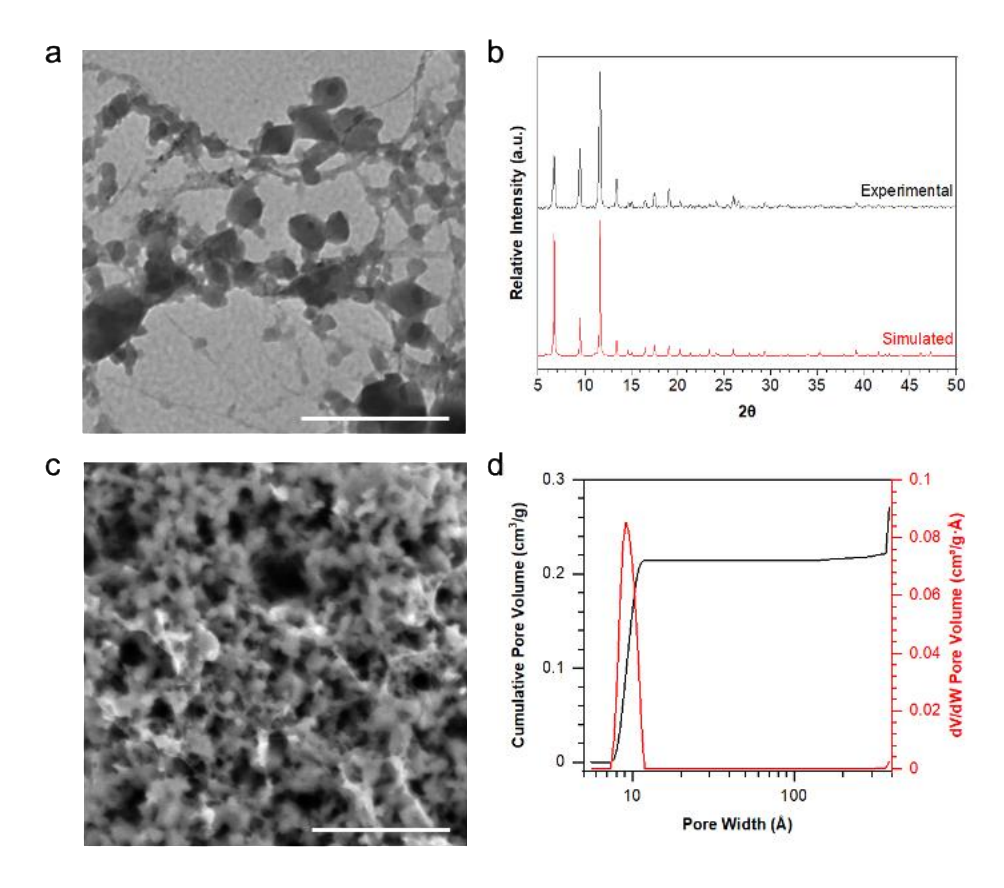


**Figure 1.** Physical characterization of the HKUST-1/Pd NP/SWCNT (a) TEM micrograph (scale bar 400 nm). (b) XRD spectra. (c) SEM micrograph (scale bar = 1 μm). (d) Cumulative pore volume and pore size distribution.

# **Hydrogen Adsorption and Desorption Sensing**

The bulk synthesized palladium nanoparticle functionalized nanotubes showed sensitivity to ppm level of hydrogen with a calculated limit of detection (S/N = 3) of  $0.52 \pm 0.11$  ppm. The devices with HKUST-1 functionalized Pd NP/SWCNT showed the higher sensitivity to hydrogen as the devices showed a larger drop in current when exposed to hydrogen (Figure 2b). This improvement in sensitivity can be explained by previous work done by Li *et. al.*, <sup>40</sup> which showed that functionalizing HKUST-1 around Pd nanocubes increased hydrogen storage capacity by 74% and improved the adsorption and desorption kinetics. Follow on experimental and theoretical work

by Chen *et. al.* showed<sup>41</sup> that the enhanced absorption by Pd NP/HKUST-1 can be explained by electrons in the 4d bands of Pd transferring into the hybridized bands of Cu and O. The holes generated in the Pd 4d bands then become available to accept electrons from H 1s orbitals to form palladium hydride.

Surprisingly, there were 4 phases of response to 10 ppm of hydrogen: 1 minute of response as the current decreased, 1.5 minutes of current stabilization, an additional 1 minute of response, and the final 6.5 minutes of recovery where the sensor current unexpectedly increased. This puzzling response behavior has no clear explanation as palladium is not expected to undergo  $\alpha$  to  $\beta$  phase change until the hydrogen concentration is above 1-2 vol% (10,000-20,000 ppm).

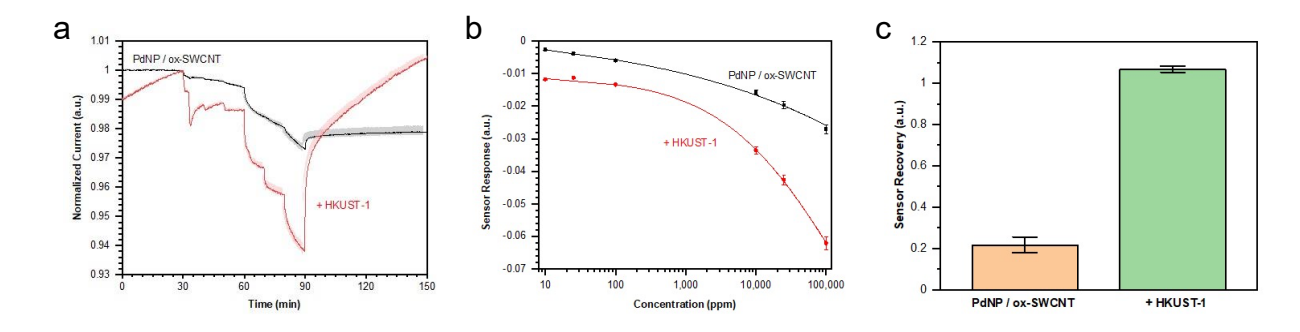


**Figure 2.** Hydrogen absorption and desorption properties of the bulk synthesized hybrid material.

(a) Hydrogen sensing characteristics of the chemireistor fabricated from the material. (b) Calibration curve of the sensing data. (c) Sensor recovery after exposure to 100,000 ppm of hydrogen.

Although the HKUST-1 functionalization increased the relative response to 10 ppm of hydrogen by more than a factor of 4 from  $0.0026 \pm 0.0002$  to  $0.0119 \pm 0.0018$ , there was a corresponding increase by more than a factor of 3 in the noise of the normalized baseline current from  $4.54 \times 10^{-5}$  to  $1.62 \times 10^{-4}$ . This corresponded to a calculated limit of detection (S/N = 3) of  $0.41 \pm 0.11$  ppm after HKUST-1 functionalization.

A substantial change in the recovery profile was observed for the HKUST-1 functionalized material (Figure 2c). The percent recovery was calculated by taking the ratio between the relative recovery from current at t = 90 minutes to t = 150 minutes to relative response to the final exposure of hydrogen at t = 90 minutes. A complete recovery of the devices to their nominal conductance would yield a value of 1.

Another noticeable trend in the sensor trace of the HKUST-1 functionalized material was the constantly increasing baseline during the nitrogen purge periods at the 0- and 90-minute marks. This baseline drift can be attributed to the ethanol desorbing from the HKUST-1 pores. Charge transfer from ethanol increases the resistance of the SWCNT, therefore desorption of ethanol will increase its conductance.<sup>43</sup>

Relative Recovery = 
$$\frac{I_{t=150} - I_{t=90}}{I_{t=30} - I_{t=90}}$$
 (1)

The average percent recovery of the devices with HKUST-1 after 60 minutes of purging with nitrogen was  $1.067 \pm 0.015$  compared to devices with only Pd/SWCNT, which was  $0.2136 \pm 0.0678$ . This enhanced recovery further supports the evidence that HKUST-1 functionalization around Pd NP, enhances the rate of hydrogen desorption.

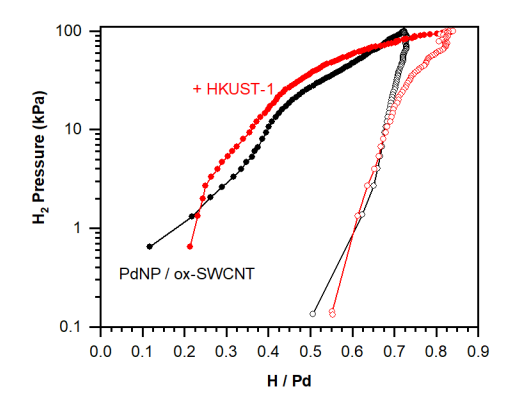


**Figure 3.** Hydrogen pressure-composition isotherms of the bulk-synthesized materials.

To correlate the improved hydrogen sensitivity of the sensors to the enhanced hydrogen absorption capacity of HKUST-1 functionalized material, pressure composition (PC) isotherms of the two materials were generated (Figure 3). The PC isotherms were obtained by converting the mass of hydrogen adsorbed per mass of material in the hydrogen adsorption isotherms (Figure S3) to per molar adsorption of hydrogen based on the experimentally determined palladium content of the materials. The palladium and copper composition of the materials were obtained by ICP-MS (Table S1). The PC isotherm of the HKUST-1/Pd NP/SWCNT showed higher absorption capacity of 0.84 hydrogen per palladium than 0.72 hydrogen per palladium for Pd NP/HKUST-1 as expected. The reported hydrogen adsorption by Li *et. al.* was 0.50 H per Pd for Pd NP and 0.87 H per Pd for HKUST-1 functionalized Pd NP.

A method to improve the sensitivity of SWCNT devices to an analyte is by using semiconductor-enriched SWCNT (s-SWCNT) instead of a mixture of metallic and semiconducting nanotubes. The sensors fabricated from s-SWCNT are much more sensitive to changes in their local charge environment due to greater changes in the density of states near the Fermi level. 44 Functionalizing palladium nanoparticles with s-SWCNT has previously shown to improve the sensitivity of the nanotube devices to hydrogen by an order of magnitude. 14-15 The improvement comes from formation of Schottky barrier, which forms between a metal and a semiconductor junction. 45 When hydrogen reacts with the palladium, the work function of the palladium changes and impedes the charge transfer between the metal and semiconducting nanotubes. This Schottky barrier effect results in a higher drop in conductance of devices fabricated from semiconducting SWCNT compared to mixed metallic and semiconducting SWCNT, which translates to more sensitive devices. 14, 46

To improve the sensitivity of the hybrid material to hydrogen, devices were fabricated using sorted s-SWCNT from NanoIntegris. The semiconducting nanotube content of these commercial nanotubes is greater than 99.9%. This is achieved by wrapping nanotubes that contains mixture of metallic and semiconducting tubes with poly-dodecylfluorene in toluene and precipitating out the metallic nanotubes.<sup>47</sup> Due to solvent incompatibility between toluene and the precursors for synthesizing PdNP and HKUST-1, a layer-by-layer method was used to first deposit the nanotubes on a silicon die followed by functionalization with Pd NP and HKUST-1.

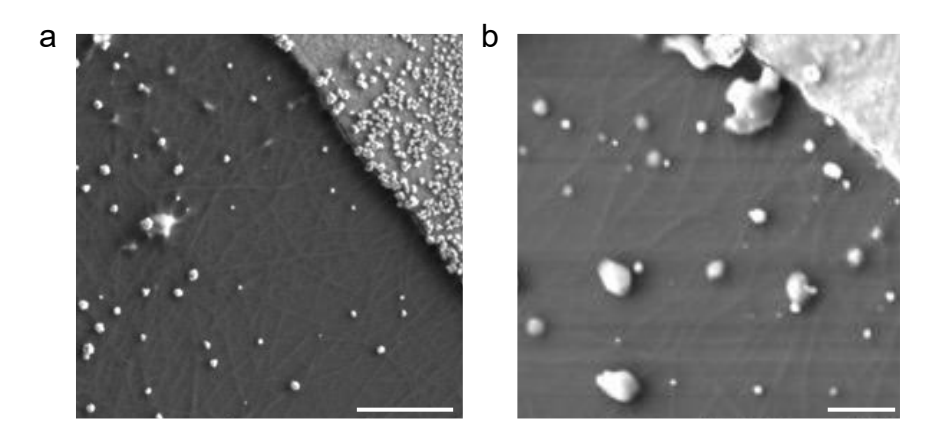


**Figure 4.** SEM micrographs of layer-by-layer synthesized hybrid material. (a) Pd NP functionalized s-SWCNT on gold electrode and silicon die (scale bar = 500 nm). (b) Post HKUST-1 functionalization.

Dielectrophoresis (DEP) was used to deposit the s-SWCNT on the silicon die followed by electrodeposition of Pd<sup>2+</sup> on the nanotubes to form Pd NP. The SEM images of the Pd NP/s-SWCNT showed a dense network of s-SWCNT deposited between the IDE (Figure 4a). On both the surfaces of the nanotubes and the gold electrode, Pd NP with sizes on the order of 5 to 50 nm with rough surfaces were observed. There was a higher density of nanoparticles on the gold electrodes due to the higher favorability of seeding and growing metal nanoparticles on a rough

metallic gold surface held at a reducing potential compared to polymer wrapped semiconducting nanotubes.

Unlike the solution-based synthesis of HKUST-1, which yielded growth of HKUST-1 around both the Pd NP and the nanotubes (Figure 4b), the layer-by-layer approach favored growth of the MOF around the Pd NP and gold electrode. Larger nanoparticles on the order of 100 to 500 nm were observed (Figure 4b). After the excess precursor solution was spun coat off the silicon die, the residual precursor solution that remained was bound to the PVP coated Pd NP and gold electrode yielding HKUST-1 growth around them.<sup>38</sup>

Pd NP functionalized s-SWCNT with and without HKUST-1 were tested for sensitivity to hydrogen. The s-SWCNT devices showed a substantial improvement in the magnitude of response to hydrogen. After 10 minutes long exposure to 10 ppm of hydrogen, the average response of 4 sensors was  $-0.054 \pm 0.010$ . The calculated LOD improved by a small margin to  $0.361 \pm 0.091$  ppm due to another factor of 4 increase in noise of the devices to  $6.441 \times 10^{-4}$  compared to the noise of HKUST-1/Pd NP/ox-SWCNT. However, the device-to-device variability also increased as the relative standard deviation of the response was  $\pm 17.9\%$ . The high variability likely can be attributed to the combination of irregular deposition of nanotubes and heterogeneous deposition of Pd NP on the nanotubes and the gold electrodes. DEP deposits nanotubes in areas of high electric

field such as the corners of the interdigitated electrodes and have high device-to-device variability. 48-49

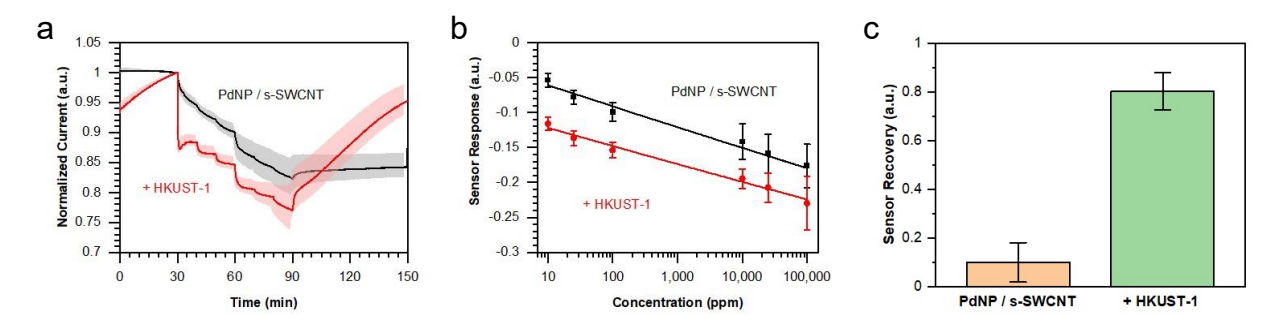


**Figure 5.** Hydrogen absorption and desorption sensing with s-SWCNT based hybrid material. (a) Hydrogen sensing characteristics of the Pd NP functionalized s-SWCNT with and without HKUST-1. (b) Calibration curve of the sensing data. (c) Sensor recovery after exposure to 100,000 ppm of hydrogen.

After the Pd NP/s-SWCNT was functionalized with HKUST-1, there was a dramatic improvement in the sensitivity of the material to hydrogen (Figure 5). The response to 10 ppm of hydrogen was  $-0.116 \pm 0.010$ , a more than a factor of 2 increase. The LOD improved by more than a factor of 5 to  $0.0700 \pm 0.010$  ppm as the noise of the devices decreased down to  $2.72 \times 10^{-4}$ . The reduction in noise may be attributed to HKUST-1 passivating the gold electrode surface. Passivating the gold electrodes with insulating materials such as polymethyl methacrylate is known to reduce device noise. Fo-51 If this LOD can be experimentally verified, it will be the best reported LOD for SWCNT based hydrogen sensor to the best of our knowledge. Table S2 in the supporting information compares the hydrogen sensing performance between the bulk and layer-by-layer synthesized materials in addition to other published works that use graphitic nanomaterials for hydrogen sensing.

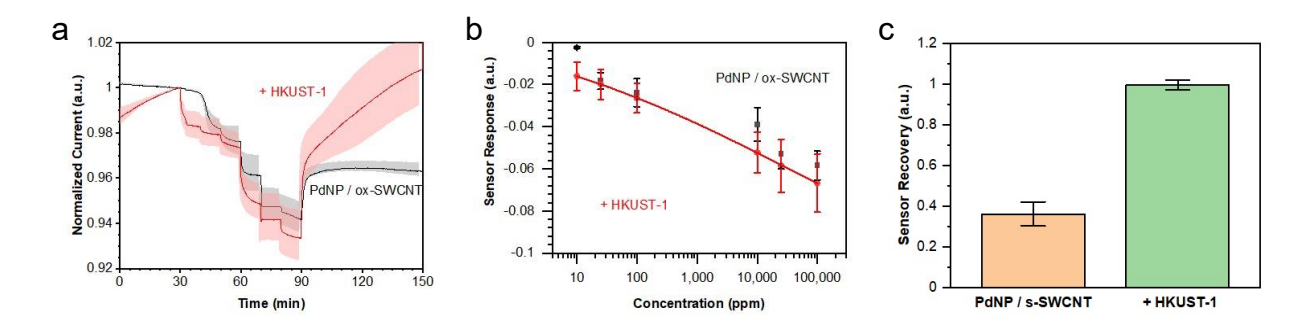


**Figure 6.** Hydrogen absorption and desorption sensing with ox-SWCNT based sensor fabricated using layer-by-layer method. (a) Hydrogen sensing characteristics of the Pd NP functionalized ox-SWCNT with and without HKUST-1. (b) Calibration curve of the sensing data. (c) Sensor recovery 60 minutes after exposure to 100,000 ppm of hydrogen.

To verify that the enriched s-SWCNT was responsible for the improvement in sensitivity to hydrogen and not the device fabrication method, the same layer-by-layer method was used to fabricate the devices from ox-SWCNT. Compared to the bulk synthesized material, the Pd NP functionalized devices did not show any response to 10 ppm of hydrogen (Figure 6). The devices instead showed a response starting from 25 ppm of hydrogen. Surprisingly, the magnitude of the response to 25 ppm of hydrogen of the LBL fabricated devices were almost twice the response of the bulk synthesized devices. After functionalization with HKUST-1, the magnitude of the response to hydrogen did not substantially increase as the error bars of the calibration curve showed large overlap pre- and post-HKUST functionalization. Again, this device-to-device variability can be attributed to DEP yielding heterogeneous coverage of deposited nanotubes. The recovery of the HKUST-1 functionalized hybrid material however did show substantially better recovery as the devices fully recovered after an hour of purging with nitrogen. Compared to the LBL fabricated mixed nanotubes-based devices, the LBL fabricated s-SWCNT based devices

show more than 7 times the response to 10 ppm of hydrogen. This direct comparison illustrates that using s-SWCNT did improve the sensitivity and LOD of the hydrogen chemiresistor.

#### Conclusion

Here we show that chemiresistor devices fabricated from HKUST-1/Pd NP functionalized SWCNT have the capability to detect the uptake and release hydrogen stored in the hybrid material. The current measured through the devices were dependent on the hydrogen concentration the nanocomposites were exposed to. The formation of palladium hydride is known to dope electrons into p-type semiconducting carbon nanotubes and decrease their conductance. HKUST-1 coating around the Pd NP increased both the storage capacity and desorption kinetics, as previously shown experimental and theoretical studies. The magnitudes of both response and recovery to hydrogen increased by after HKUST-1 functionalization.

To improve the sensitivity of the devices, semiconducting enriched carbon nanotubes were used instead of mixture of metallic and semiconducting nanotubes. Semiconducting nanotubes were expected to improve both the limit of detection and sensitivity as metallic nanotubes do not have a band gap that can be modulated by the formation palladium hydride and only contribute background current to the devices. The use of enriched s-SWCNT in the hybrid improved the calculated limit of detection to 70 ppb, which will be the best LOD reported to date if the results can be experimentally verified.

If MOF functionalized Pd NP find applications in hydrogen storage material, this work illustrates that incorporating chemiresistive devices fabricated from carbon nanotube functionalized with the same MOF and Pd NP can serve as an *in-situ* detector that provides real-time monitoring of the concentration of the stored hydrogen.

#### ASSOCIATED CONTENT

**Supporting Information.** High-resolution transmission electron microscopy, nitrogen and hydrogen adsorption isotherms, ICP-MS results, and comparison to other hydrogen sensors. This material is available free of charge via the Internet at <a href="http://pubs.acs.org">http://pubs.acs.org</a>.

#### **Author Information**

#### **Corresponding Author**

Alexander Star — Department of Chemistry and Department of Bioengineering, University of Pittsburgh, Pittsburgh, Pennsylvania 15260, United States; <u>orcid.org/0000-0001-7863-5987</u>; Email: astar@pitt.edu

#### Authors

**Sean I. Hwang** — Department of Chemistry, University of Pittsburgh, Pittsburgh, Pennsylvania 15260, United States

Emmy M. Sopher — Department of Chemistry, University of Pittsburgh, Pittsburgh, Pennsylvania 15260, United States

**Zidao Zeng** — Department of Chemistry, University of Pittsburgh, Pittsburgh, Pennsylvania 15260, United States

Zachary M. Schulte — Department of Chemistry, University of Pittsburgh, Pittsburgh, Pennsylvania 15260, United States; orcid.org/0000-0002-9189-6265

**David L. White** — Department of Chemistry, University of Pittsburgh, Pittsburgh, Pennsylvania 15260, United States

Nathaniel L. Rosi — Department of Chemistry and Department of Chemical & Petroleum Engineering, University of Pittsburgh, Pittsburgh, Pennsylvania 15260, United States; orcid.org/0000-0001-8025-8906

## Acknowledgement

The work was supported by the National Science Foundation under Grant No. 2003302. The authors thank the Nanoscale Fabrication and Characterization Facility of the Peterson Institute of Nanoscience and Engineering for access to characterization instrumentation and Susheng Tan for assistance with the execution of this part of our research.

#### References

- (1) Rowsell, J. L.; Spencer, E. C.; Eckert, J.; Howard, J. A.; Yaghi, O. M. Gas adsorption sites in a large-pore metal-organic framework. *Science* **2005**, *309* (5739), 1350-4, DOI: 10.1126/science.1113247.
- (2) Li, J. R.; Kuppler, R. J.; Zhou, H. C. Selective gas adsorption and separation in metal-organic frameworks. *Chem. Soc. Rev.* **2009**, *38* (5), 1477-504, DOI: 10.1039/b802426j.
- (3) Freund, R.; Zaremba, O.; Arnauts, G.; Ameloot, R.; Skorupskii, G.; Dinca, M.; Bavykina, A.; Gascon, J.; Ejsmont, A.; Goscianska, J.; Kalmutzki, M.; Lachelt, U.; Ploetz, E.; Diercks, C. S.; Wuttke, S. The Current Status of MOF and COF Applications. *Angew. Chem. Int. Ed. Engl.* **2021**, *60* (45), 23975-24001, DOI: 10.1002/anie.202106259.
- (4) Farha, O. K.; Yazaydin, A. O.; Eryazici, I.; Malliakas, C. D.; Hauser, B. G.; Kanatzidis, M. G.; Nguyen, S. T.; Snurr, R. Q.; Hupp, J. T. De novo synthesis of a metal-organic framework material featuring ultrahigh surface area and gas storage capacities. *Nat. Chem.* **2010**, *2* (11), 944-8, DOI: 10.1038/nchem.834.
- (5) Gascon, J.; Corma, A.; Kapteijn, F.; Llabrés i Xamena, F. X. Metal Organic Framework Catalysis: Quo vadis? *ACS Catal.* **2013**, *4* (2), 361-378, DOI: 10.1021/cs400959k.
- (6) Rodenas, T.; Luz, I.; Prieto, G.; Seoane, B.; Miro, H.; Corma, A.; Kapteijn, F.; Llabres, I. X. F. X.; Gascon, J. Metal-organic framework nanosheets in polymer composite materials for gas separation. *Nat. Mater.* **2015**, *14* (1), 48-55, DOI: 10.1038/nmat4113.
- (7) Kreno, L. E.; Leong, K.; Farha, O. K.; Allendorf, M.; Van Duyne, R. P.; Hupp, J. T. Metalorganic framework materials as chemical sensors. *Chem. Rev.* **2012**, *112* (2), 1105-25, DOI: 10.1021/cr200324t.
- (8) Li, H. Y.; Zhao, S. N.; Zang, S. Q.; Li, J. Functional metal-organic frameworks as effective sensors of gases and volatile compounds. *Chem. Soc. Rev.* **2020**, *49* (17), 6364-6401, DOI: 10.1039/c9cs00778d.
- (9) Li, Y.; Yang, R. T. Gas adsorption and storage in metal-organic framework MOF-177. *Langmuir* **2007**, *23* (26), 12937-44, DOI: 10.1021/la702466d.
- (10) Zhang, Y. B.; Furukawa, H.; Ko, N.; Nie, W.; Park, H. J.; Okajima, S.; Cordova, K. E.; Deng, H.; Kim, J.; Yaghi, O. M. Introduction of functionality, selection of topology, and enhancement of gas adsorption in multivariate metal-organic framework-177. *J. Am. Chem. Soc.* **2015,** *137* (7), 2641-50, DOI: 10.1021/ja512311a.

- (11) Yang, S.; Lin, X.; Blake, A. J.; Walker, G. S.; Hubberstey, P.; Champness, N. R.; Schroder, M. Cation-induced kinetic trapping and enhanced hydrogen adsorption in a modulated anionic metal-organic framework. *Nat. Chem.* **2009**, *1* (6), 487-93, DOI: 10.1038/nchem.333.
- (12) Kong, J.; Chapline, M. G.; Dai, H. Functionalized Carbon Nanotubes for Molecular Hydrogen Sensors. *Adv. Mater.* **2001**, *13* (18), 1384-1386, DOI: 10.1002/1521-4095(200109)13:18<1384::Aid-adma1384>3.0.Co;2-8.
- (13) Mubeen, S.; Zhang, T.; Yoo, B.; Deshusses, M. A.; Myung, N. V. Palladium Nanoparticles Decorated Single-Walled Carbon Nanotube Hydrogen Sensor. *J. Phys. Chem. C* **2007**, *111* (17), 6321-6327, DOI: 10.1021/jp067716m.
- (14) Ganzhorn, M.; Vijayaraghavan, A.; Dehm, S.; Hennrich, F.; Green, A. A.; Fichtner, M.; Voigt, A.; Rapp, M.; von Lohneysen, H.; Hersam, M. C.; Kappes, M. M.; Krupke, R. Hydrogen sensing with diameter- and chirality-sorted carbon nanotubes. *ACS Nano* **2011**, *5* (3), 1670-6, DOI: 10.1021/nn101992g.
- (15) Xiao, M.; Liang, S.; Han, J.; Zhong, D.; Liu, J.; Zhang, Z.; Peng, L. Batch Fabrication of Ultrasensitive Carbon Nanotube Hydrogen Sensors with Sub-ppm Detection Limit. *ACS Sens.* **2018**, *3* (4), 749-756, DOI: 10.1021/acssensors.8b00006.
- (16) Collins, P. G.; Bradley, K.; Ishigami, M.; Zettl, A. Extreme oxygen sensitivity of electronic properties of carbon nanotubes. *Science* **2000**, *287* (5459), 1801-4, DOI: 10.1126/science.287.5459.1801.
- (17) Kong, J.; Franklin, N. R.; Zhou, C. W.; Chapline, M. G.; Peng, S.; Cho, K. J.; Dai, H. J. Nanotube molecular wires as chemical sensors. *Science* **2000**, *287* (5453), 622-625, DOI: 10.1126/science.287.5453.622.
- (18) Chen, R. J.; Choi, H. C.; Bangsaruntip, S.; Yenilmez, E.; Tang, X.; Wang, Q.; Chang, Y. L.; Dai, H. An investigation of the mechanisms of electronic sensing of protein adsorption on carbon nanotube devices. *J. Am. Chem. Soc.* **2004**, *126* (5), 1563-8, DOI: 10.1021/ja038702m.
- (19) Lee, C. Y.; Strano, M. S. Understanding the dynamics of signal transduction for adsorption of gases and vapors on carbon nanotube sensors. *Langmuir* **2005**, *21* (11), 5192-6, DOI: 10.1021/la046867i.
- (20) Ding, M.; Tang, Y.; Star, A. Understanding Interfaces in Metal-Graphitic Hybrid Nanostructures. *J. Phys. Chem. Lett.* **2013**, *4* (1), 147-60, DOI: 10.1021/jz301711a.
- (21) Ding, M.; Sorescu, D. C.; Star, A. Photoinduced charge transfer and acetone sensitivity of single-walled carbon nanotube-titanium dioxide hybrids. *J. Am. Chem. Soc.* **2013**, *135* (24), 9015-22, DOI: 10.1021/ja402887v.
- (22) Li, X.; Le Thai, M.; Dutta, R. K.; Qiao, S.; Chandran, G. T.; Penner, R. M. Sub-6 nm Palladium Nanoparticles for Faster, More Sensitive H2 Detection Using Carbon Nanotube Ropes. *ACS Sens.* **2017**, *2* (2), 282-289, DOI: 10.1021/acssensors.6b00808.
- (23) Miner, E. M.; Fukushima, T.; Sheberla, D.; Sun, L.; Surendranath, Y.; Dinca, M. Electrochemical oxygen reduction catalysed by Ni3(hexaiminotriphenylene)2. *Nat. Commun.* **2016,** *7*, 10942, DOI: 10.1038/ncomms10942.
- (24) Meng, Z.; Stolz, R. M.; Mendecki, L.; Mirica, K. A. Electrically-Transduced Chemical Sensors Based on Two-Dimensional Nanomaterials. *Chem. Rev.* **2019**, *119* (1), 478-598, DOI: 10.1021/acs.chemrev.8b00311.
- (25) Campbell, M. G.; Sheberla, D.; Liu, S. F.; Swager, T. M.; Dinca, M. Cu(3)(hexaiminotriphenylene)(2): an electrically conductive 2D metal-organic framework for chemiresistive sensing. *Angew. Chem. Int. Ed. Engl.* **2015**, *54* (14), 4349-52, DOI: 10.1002/anie.201411854.

- (26) Ko, M.; Mendecki, L.; Eagleton, A. M.; Durbin, C. G.; Stolz, R. M.; Meng, Z.; Mirica, K. A. Employing Conductive Metal-Organic Frameworks for Voltammetric Detection of Neurochemicals. *J. Am. Chem. Soc.* **2020**, *142* (27), 11717-11733, DOI: 10.1021/jacs.9b13402. (27) Xie, L. S.; Skorupskii, G.; Dinca, M. Electrically Conductive Metal-Organic Frameworks. *Chem. Rev.* **2020**, *120* (16), 8536-8580, DOI: 10.1021/acs.chemrev.9b00766.
- (28) Ellis, J. E.; Zeng, Z.; Hwang, S. I.; Li, S.; Luo, T. Y.; Burkert, S. C.; White, D. L.; Rosi, N. L.; Gassensmith, J. J.; Star, A. Growth of ZIF-8 on molecularly ordered 2-methylimidazole/single-walled carbon nanotubes to form highly porous, electrically conductive composites. *Chem. Sci.* **2019**, *10* (3), 737-742, DOI: 10.1039/c8sc03987a.
- (29) Zeng, Z.; Sorescu, D. C.; White, D. L.; Hwang, S. I.; Shao, W.; He, X.; Schulte, Z. M.; Rosi, N. L.; Star, A. Heterogeneous Growth of UiO-66-NH2 on Oxidized Single-Walled Carbon Nanotubes to Form "Beads-on-a-String" Composites. *ACS Appl. Mater. Interfaces* **2021**, *13* (13), 15482-15489, DOI: 10.1021/acsami.0c21509.
- (30) Yoo, J.; Lee, S.; Lee, C. K.; Kim, C.; Fujigaya, T.; Park, H. J.; Nakashima, N.; Shim, J. K. Homogeneous decoration of zeolitic imidazolate framework-8 (ZIF-8) with core—shell structures on carbon nanotubes. *RSC Adv.* **2014**, *4* (91), 49614-49619, DOI: 10.1039/c4ra06792d.
- (31) White, D. L.; Day, B. A.; Zeng, Z.; Schulte, Z. M.; Borland, N. R.; Rosi, N. L.; Wilmer, C. E.; Star, A. Size Discrimination of Carbohydrates via Conductive Carbon Nanotube@Metal Organic Framework Composites. *J. Am. Chem. Soc.* **2021**, *143* (21), 8022-8033, DOI: 10.1021/jacs.1c01673.
- (32) Saini, H.; Srinivasan, N.; Sedajova, V.; Majumder, M.; Dubal, D. P.; Otyepka, M.; Zboril, R.; Kurra, N.; Fischer, R. A.; Jayaramulu, K. Emerging MXene@Metal-Organic Framework Hybrids: Design Strategies toward Versatile Applications. *ACS Nano* **2021**, *15* (12), 18742-18776, DOI: 10.1021/acsnano.1c06402.
- (33) Wang, D.; Zhang, D.; Yang, Y.; Mi, Q.; Zhang, J.; Yu, L. Multifunctional Latex/Polytetrafluoroethylene-Based Triboelectric Nanogenerator for Self-Powered Organ-like MXene/Metal-Organic Framework-Derived CuO Nanohybrid Ammonia Sensor. *ACS Nano* **2021**, *15* (2), 2911-2919, DOI: 10.1021/acsnano.0c09015.
- (34) Prasanth, K. P.; Rallapalli, P.; Raj, M. C.; Bajaj, H. C.; Jasra, R. V. Enhanced hydrogen sorption in single walled carbon nanotube incorporated MIL-101 composite metal—organic framework. *Int. J. Hydrogen Energy* **2011**, *36* (13), 7594-7601, DOI: 10.1016/j.ijhydene.2011.03.109.
- (35) Cortes-Suarez, J.; Celis-Arias, V.; Beltran, H. I.; Tejeda-Cruz, A.; Ibarra, I. A.; Romero-Ibarra, J. E.; Sanchez-Gonzalez, E.; Loera-Serna, S. Synthesis and Characterization of an SWCNT@HKUST-1 Composite: Enhancing the CO2 Adsorption Properties of HKUST-1. *ACS Omega* **2019**, *4* (3), 5275-5282, DOI: 10.1021/acsomega.9b00330.
- (36) Singh, P.; Kulkarni, M. V.; Gokhale, S. P.; Chikkali, S. H.; Kulkarni, C. V. Enhancing the hydrogen storage capacity of Pd-functionalized multi-walled carbon nanotubes. *Appl. Surf. Sci.* **2012**, *258* (8), 3405-3409, DOI: 10.1016/j.apsusc.2011.11.075.
- (37) Chen, A.; Ostrom, C. Palladium-Based Nanomaterials: Synthesis and Electrochemical Applications. *Chem. Rev.* **2015**, *115* (21), 11999-2044, DOI: 10.1021/acs.chemrev.5b00324.
- (38) Zhuang, J.-L.; Ceglarek, D.; Pethuraj, S.; Terfort, A. Rapid Room-Temperature Synthesis of Metal-Organic Framework HKUST-1 Crystals in Bulk and as Oriented and Patterned Thin Films. *Adv. Funct. Mater.* **2011**, *21* (8), 1442-1447, DOI: 10.1002/adfm.201002529.
- (39) Quinn, B. M.; Dekker, C.; Lemay, S. G. Electrodeposition of noble metal nanoparticles on carbon nanotubes. *J. Am. Chem. Soc.* **2005**, *127* (17), 6146-7, DOI: 10.1021/ja0508828.

- (40) Li, G.; Kobayashi, H.; Taylor, J. M.; Ikeda, R.; Kubota, Y.; Kato, K.; Takata, M.; Yamamoto, T.; Toh, S.; Matsumura, S.; Kitagawa, H. Hydrogen storage in Pd nanocrystals covered with a metal-organic framework. *Nat. Mater.* **2014**, *13* (8), 802-6, DOI: 10.1038/nmat4030.
- (41) Chen, Y.; Sakata, O.; Nanba, Y.; Kumara, L. S. R.; Yang, A.; Song, C.; Koyama, M.; Li, G.; Kobayashi, H.; Kitagawa, H. Electronic origin of hydrogen storage in MOF-covered palladium nanocubes investigated by synchrotron X-rays. *Commun. Chem* **2018**, *I* (1), 61, DOI: 10.1038/s42004-018-0058-3.
- (42) Favier, F.; Walter, E. C.; Zach, M. P.; Benter, T.; Penner, R. M. Hydrogen sensors and switches from electrodeposited palladium mesowire arrays. *Science* **2001**, *293* (5538), 2227-31, DOI: 10.1126/science.1063189.
- (43) Brahim, S.; Colbern, S.; Gump, R.; Moser, A.; Grigorian, L. Carbon nanotube-based ethanol sensors. *Nanotechnology* **2009**, *20* (23), 235502, DOI: 10.1088/0957-4484/20/23/235502.
- (44) Guo, C.; Ouyang, J.; Shin, H.; Ding, J.; Li, Z.; Lapointe, F.; Lefebvre, J.; Kell, A. J.; Malenfant, P. R. L. Enrichment of Semiconducting Single-Walled Carbon Nanotubes with Indigo-Fluorene-Based Copolymers and Their Use in Printed Thin-Film Transistors and Carbon Dioxide Gas Sensors. *ACS Sens.* **2020**, *5* (7), 2136-2145, DOI: 10.1021/acssensors.0c00764.
- (45) Tung, R. T. The physics and chemistry of the Schottky barrier height. *Appl. Phys. Rev.* **2014**, *I* (1), 011304, DOI: 10.1063/1.4858400.
- (46) Zhang, M.; Brooks, L. L.; Chartuprayoon, N.; Bosze, W.; Choa, Y. H.; Myung, N. V. Palladium/single-walled carbon nanotube back-to-back Schottky contact-based hydrogen sensors and their sensing mechanism. *ACS Appl. Mater. Interfaces* **2014**, *6* (1), 319-26, DOI: 10.1021/am404328g.
- (47) Ding, J.; Li, Z.; Lefebvre, J.; Cheng, F.; Dubey, G.; Zou, S.; Finnie, P.; Hrdina, A.; Scoles, L.; Lopinski, G. P.; Kingston, C. T.; Simard, B.; Malenfant, P. R. Enrichment of large-diameter semiconducting SWCNTs by polyfluorene extraction for high network density thin film transistors. *Nanoscale* **2014**, *6* (4), 2328-39, DOI: 10.1039/c3nr05511f.
- (48) Hu, L.; Hecht, D. S.; Gruner, G. Carbon nanotube thin films: fabrication, properties, and applications. *Chem. Rev.* **2010**, *110* (10), 5790-5844, DOI: 10.1021/cr9002962.
- (49) Chen, J.; Kumar, S. Variability in Output Characteristics of Single-Walled Carbon Nanotube Thin-Film Transistors. *IEEE Trans. Nanotechnol.* **2018**, *17* (2), 353-361, DOI: 10.1109/tnano.2018.2803106.
- (50) Peng, N.; Zhang, Q.; Chow, C. L.; Tan, O. K.; Marzari, N. Sensing mechanisms for carbon nanotube based NH3 gas detection. *Nano Lett.* **2009**, *9* (4), 1626-30, DOI: 10.1021/nl803930w.
- (51) Heller, I.; Mannik, J.; Lemay, S. G.; Dekker, C. Optimizing the signal-to-noise ratio for biosensing with carbon nanotube transistors. *Nano Lett.* **2009**, *9* (1), 377-82, DOI: 10.1021/nl8031636.

# Table of Contents Graphic

